

General Disclaimer

One or more of the Following Statements may affect this Document

- This document has been reproduced from the best copy furnished by the organizational source. It is being released in the interest of making available as much information as possible.
- This document may contain data, which exceeds the sheet parameters. It was furnished in this condition by the organizational source and is the best copy available.
- This document may contain tone-on-tone or color graphs, charts and/or pictures, which have been reproduced in black and white.
- This document is paginated as submitted by the original source.
- Portions of this document are not fully legible due to the historical nature of some of the material. However, it is the best reproduction available from the original submission.

X-625-71-258

FREPRINT

NASA TM X- 65651

**POSITIVE ION COMPOSITION
MEASUREMENTS IN THE
D & E REGIONS
OF THE EQUATORIAL IONOSPHERE**

FACILITY FORM 602

(ACCESSION NUMBER)

23

(PAGES)

N71-325011
TMX-65651

(NASA CR OR TMX OR AD NUMBER)

G3

(CODE)

13

(CATEGORY)

RICHARD A. GOLDBERG

JULY 1971

GSFC

**GODDARD SPACE FLIGHT CENTER
GREENBELT, MARYLAND**

For Presentation at the COSPAR Symposium on
D & E Region Ion Chemistry, Urbana, Illinois,
July 6-8, 1971

POSITIVE ION COMPOSITION MEASUREMENTS IN THE D
AND E REGIONS OF THE EQUATORIAL IONOSPHERE

by

Richard A. Goldberg
Laboratory for Planetary Atmospheres
Chemosphere Branch
NASA/Goddard Space Flight Center
Greenbelt, Maryland

For presentation at the COSPAR Symposium on D and E-Region Ion Chemistry, Urbana, Illinois, July 6-8, 1971.

POSITIVE ION COMPOSITION MEASUREMENTS IN THE D
AND E REGIONS OF THE EQUATORIAL IONOSPHERE

by

Richard A. Goldberg
Laboratory for Planetary Atmospheres
NASA/Goddard Space Flight Center
Greenbelt, Maryland

1. INTRODUCTION

We present here some positive ion composition results obtained from rocket measurements made at Thumba, India (magnetic dip = -1.7°) on March 19, 1970 for solar zenith angles of 53.2 and 27.8° . The composition was measured using quadrupole ion mass spectrometers housed in titanium getter pumped systems similar to the one described by Goldberg and Blumle [1]. D region measurements were carried out during both upleg ram and downleg wake sampling conditions for each flight. Also included in the payloads were experiments to measure positive ion and electron concentrations, Lyman alpha radiation, and the $2\text{-}8 \text{ \AA}$ solar X-ray spectrum. The results of these latter experiments are partially discussed herein but are reported in detail elsewhere [2].

Evidence is presented for the breakdown of D region ambient heavy cluster ions to 37^+ and possibly 19^+ by shock wave effects induced by the rocket motion. A qualitative comparison is made between the observed positive ion composition measured under ram and under weak

shock (downleg wake) conditions leading to the conclusion that wake data is more reliable as an ambient sample in the D region.

The equatorial E region is studied on the same two rocket flights up to altitudes approaching 125 km. Two additional rockets with similar instrumentation were flown on the night of March 9-10, 1970 and provide nighttime E region data for comparison with the daytime results.

2. EXPERIMENTAL DESCRIPTION

Each payload contained a quadrupole ion mass spectrometer housed in a titanium getter pumped system assisted by two triode ion pumps for inert gas pumping. The details of this system plus the performance characteristics are described in Goldberg and Aikin [3].

The daytime flights also contained radio absorption experiments [4] at 1.865 and 3.030 MHz to determine electron density and Gerdien probes for determination of positive ion density [2]. The electron density profiles at night were determined using a continuous wave dispersive Doppler experiment [5], [6], [7] at frequencies of 73.6 and 24.53 MHz. Spectrometer currents were normalized to the electron density profiles to determine absolute values of ion species.

D region data from both ram and wake sampling configurations are presented in this work. By detaching the rocket

payload during the upleg portion of the flight, a fixed attitude is obtained to heights below 65 km on downleg. This permits upleg ram sampling to be directly compared with downleg wake sampling at D region altitudes.

3. D REGION RESULTS

3.1 Shock Wave Effects

Typical raw spectra from one of the daytime rockets (NASA 14.424) are illustrated in Figure 1. These data are presented with the currents displayed on a logarithmic scale (ordinate) in which each volt above one volt represents a full decade of sensitivity; below one volt, the scale is nearly linear.

Both upleg and downleg spectra are illustrated for the same altitude range from 82 to 85 km. We observe no apparent loss of sensitivity induced by wake sampling in this region. The flat curves labelled "total" at the right of each spectrum are total current measurements during high pass filter mode operation of the instrument. They indicate the relative contribution of heavy constituents beyond the sweep range of the instrument to the total current. It is apparent that the downleg portion of the flight exhibits much stronger contributions from the heavy constituents (48^+ , 55^+ , $> 65^+$) than observed on upleg.

Figure 2 traces the raw current ratio of heavy constituents (I_B) to total constituents during up and downleg of 14.424 as obtained from the high pass filter mode data. An enhancement of this ratio thereby implies a

greater contribution of heavy constituents to the total current. Of note is the uniform value of this ratio between up and downleg in the metallic region (90-110 km) where the major contribution to I_B is iron (56^+). The lack of change between up and downleg in this region suggests that heavy constituents are either metallic atomic ions and hence unaffected by shock effects, or of another origin unperturbed by the relatively weak shocks there. Below 85 km, designated the water cluster region, an enhancement of nearly 10 is observed for the ratio, indicating a much greater contribution of heavy water cluster constituents in the wake sampling region than in that of the ram. These heavier clusters are known to have low energies of dissociation leading to the suggestion that shock wave temperature and pressure effects are sufficient to induce breakup of these heavier clusters into lighter clusters [8], [9]. The evidence here appears to verify this suggestion because under ram conditions, sampling occurs much closer to that portion of the shock where ambient ions have been subjected to maximum pressures and temperatures. A certain percentage of such ions should also flow into the wake region, but a much higher proportion of particles sampled in the wake will have traversed across weaker portions of the shock at lower pressures, where conditions for dissociation are much less probable.

Figure 3 compares the upleg and downleg reduced absolute ion composition profiles for the D region portion of flight 14.424. The enhanced contributions of 48^+ , 55^+ , and T_B ($M^+ > 65^+$) in the downleg portion of the flight specify the constituents contributing to the effect observed in Figure 2.

We also note that rocket 14.424 passed through the D region at Mach 3.2. An earlier rocket on the same day (NASA 14.425, Figure 4) passed through the same region at Mach 2.2. We observe a larger contribution of heavy water cluster constituents to the upleg data than seen on 14.424. Finally, we note that on rockets traveling through the D region at Mach 6-7 we have observed a complete absence of the heavy water cluster constituents [1]. Both of these results further imply that slower moving vehicles with weaker shocks should permit data acquisition under more nearly ambient conditions.

3.2 Results and Discussion

The normalized positive ion composition profiles are illustrated in Figures 3 and 4 for 14.424 and 14.425, respectively. The curve marked T_B represents the sum of all mass to charge ratios for $M > 65$. In this work all ions are assumed to be singly ionized for identification purposes.

The data illustrated in Figures 3 and 4 were obtained by normalizing the ion composition currents to

total density profiles obtained from the Gerdien and radio propagation experiments. No mass dependent corrections were made with regard to free molecular flow, since evidence exists that such severe mass dependent corrections are improper below 90 km. The actual details of this data reduction are reported elsewhere [3]. Care should be taken in the quantitative interpretation of the downleg data for 14.425, since pump operating pressures were much higher than normal. Below 75 km on both flights, the currents measured were quite small, causing measurements to be made near the maximum sensitivity limits of the instrument. The data is thought to be reliable in this height range on a qualitative basis only.

From the previous discussion it is clear that modifications due to shock effects occur in the sampling of ion spectra with rocket-borne ion spectrometers at D region altitudes. It is however, possible to develop a qualitative picture of the species and their distribution. A quantitative analysis will require ion mass spectrometer sampling at subsonic velocities.

The downleg ion density profiles from rocket 14.424 (Figure 3) show the primary ion below 83 km to be 37^+ with 55^+ and 30^+ appearing as major ionic constituents. The hydronium ion, 19^+ , as well as 48^+ are secondary ions.

The distribution of 55^+ follows that of 30^+ . In addition, the peaks of 55^+ , 48^+ , and 30^+ occur at 77 km, which is also the measured peak of production of NO^+ (30^+) by solar Lyman alpha radiation; thus indicating that these ions originate from this ionization source. Above 83 km there is a sudden decrease in the hydrated ion cluster densities coinciding with the increase in electron density in the lower E region of the ionosphere.

The data of 14.425 (Figure 4) are not as good in quality as those of 14.424 so that care should be taken in reading as much into the 14.425 profiles. It should be noted however, that in this data 37^+ is no longer the dominant constituent; instead, 30^+ predominates. Ions of secondary importance are 37^+ and $M^+ > 65^+$.

Above 80 km, the increased height of X-ray unit optical depth in conjunction with X-rays as a primary source of O_2^+ is consistent with the reduced 37^+ at larger solar zenith angles. Below 80 km, certain inconsistencies occur related to our current lack of knowledge concerning minor constituents, reactions, reaction rates, and other sources of water cluster ions in this region. A more detailed analysis of this data is presented in [3].

4. E REGION RESULTS

In this section we present upleg data from 85 to 125 km for four independent rocket flights, all fired during March, 1970. The daytime Nike Apache flights (NASA 14.425 and 14.424) are the upper portion of the D region flights already

discussed in the previous sections. The nighttime Nike Tomahawk flights (NASA 18.97 and 18.98) occurred during the night of March 9-10 at 19:38 and 1:08 LMT. Data for each of these flights were obtained to 300 km, but only the E region results in the domain comparable with daytime data will be discussed here. The absolute density profiles on the nighttime flights were obtained by normalization to the profile obtained from the previously discussed dispersive Doppler CW propagation experiment. Above 90 km, normalization procedures included mass weighting based on free molecular flow effects.

Turning first to the daytime data illustrated in Figure 5, $30^+(\text{NO}^+)$ and $32^+(\text{O}_2^+)$ are the major constituents. It is interesting to observe oscillations among the major constituents. However, it is not immediately apparent as to what type of mechanism would operate to produce opposite phasing between 30^+ and 32^+ as a function of altitude. The structure shown for the most minor constituents are partially real but are also induced by the increased errors when operating near the extreme sensitivity limits of the instruments.

The metallic belt appears to maximize near 93 km at a density of 400 cm^{-3} and is dominated by Mg^+ and Fe^+ . Smaller concentrations of Na^+ , Al^+ , Si^+ , K^+ and Ca^+ are also observed. Important minor isotopes of the above constituents are observed but not shown. The minor constituents are

less apparent in the data of 14.425 because of inferior operating conditions for this instrument. This may also account in part for the apparent depletion in 24^+ below 90 km on this flight.

From the daytime data, we conclude that the metallic layers are well defined at the magnetic equator, although perhaps of broader peak width than at midlatitudes [10], [11], [12]. Above 100 km a low trace background of metallics occurs up to apogee, with no secondary ledges of metal ions in the 110 km range as observed at midlatitudes.

The nighttime data are illustrated in Figure 6. Here, height resolution is poorer because of sampling aboard higher speed vehicles. The spectrometer sweep range for the nighttime flights did not exceed 42^+ , so that Fe^+ must be approximated by the T_B curve. Also, the spectrometer aboard 18.97 had lower sensitivity than that aboard 18.98.

First, we note that the observed metallic belt in the data of 18.97 exhibits a broad peak width centered about 98 km with a peak density near 10^3 cm^{-3} . This larger density at night may partially be accounted for by the 10 day difference between day and night data sampling, and by the different techniques used to obtain total density. The 18.97 data were obtained under postsunset conditions when the F layer had reached a peak altitude of 550 km as determined from ionogram analysis. The data of 18.98 were obtained after

the F layer had drifted downward to a height near 300 km. At this time, the metallic layer is observed to be more pronounced, with properties quite similar to the daytime case but for a peak density over twice as large. There is no evidence for sporadic E on ionograms recorded during either of the two flights.

Awe [13] has recently reported that the equatorial sporadic E virtual height ($h'E_S$) exhibits an in-phase correlation with the postsunset drift induced height shift of the equatorial F layer. Typical E_S drifts occur between 1-3 m/s with a reduced effect under magnetically disturbed conditions. The data presented here illustrates that the equatorial metallic layer is subjected to similar drifts, induced by dynamo electric fields. The magnitude of the observed displacement (5 km) can be accounted for by an average downward drift just under 1 m/s, which correlates nicely with the fact that the night of March 9-10 was moderately disturbed with K_p 's in the 4-6 range.

The height of the nighttime metallic layer coincides with a depletion of NO^+ and O_2^+ , an effect most pronounced in the data of 18.98. This effect is masked in the daytime by the much larger concentrations of NO^+ and O_2^+ present. The metallic peak seems to be relatively insensitive to daytime photoionization effects, in the sense that the

daytime layer appears reasonably unmodified from the nighttime shape and size. These two observations suggest charge transfer of NO^+ and O_2^+ with metallic neutral constituents to be of primary importance in the formation of the equatorial metallic ion layer, especially for the major constituents Mg^+ and Fe^+ . This interpretation concurs with the conclusions of Narcisi [11] and Swider [14] that charge exchange processes do indeed dominate photoionization in the production of these constituents.

Finally, we note no obvious perturbation in the ion composition induced by the equatorial electrojet. The flight of 14.424 occurred within an hour of the expected maximum for the daytime electrojet, anticipated to be at altitudes from 105 to 115 km [15], [16].

5. CONCLUSION

The equatorial D region positive ion composition has been studied with two rocket payloads launched at Thumba India on March 19, 1970. The observed distribution indicates no major variations from the measured midlatitude distribution. The data exhibits strong shock effects under ram sampling in the sense that heavy water clusters are dissociated to lighter mass values. Hence, wake sampled data is believed to provide a more realistic description of the ambient D region than ram sampled data.

The D region wake data has provided certain qualitative results. The midday equatorial D region is observed

to be dominated by 37^+ . Heavy water clusters (48^+ , 55^+ , $>65^+$) peak at the Lyman alpha unit optical depth, suggesting NO^+ as a major source for these constituents.

The reduction of 37^+ to secondary status at high zenith angle is observed. The larger zenith angle leads to the reduction of X-ray penetration into the D region, consistent with the interpretation for the distribution above 80 km. However, this cannot account for the distribution below this height on the basis of currently accepted parameters and reactions.

The same two rocket flights provide E region data up to an altitude approaching 125 km. This is compared with the E region ion composition observed on two nighttime rocket flights ten days earlier. We observe that the daytime equatorial E region is dominated by NO^+ and O_2^+ as expected. These are found to oscillate with height, out of phase with each other.

The equatorial E region contains a metallic belt centered at 93 km and dominated by Mg^+ and Fe^+ . Traces of Na^+ , Al^+ , Si^+ , K^+ and Ca^+ are also detected. The layer has a broader peak width and the metallics show no secondary maxima above 100 km as observed at midlatitudes. We find this metallic layer to exhibit a postsunset rise followed by a downward drift to normal height by 1:08 LMT, indicating an in-phase relationship with the nighttime

dynamo controlled $h'E_S$ and h_mF2 drifts.

An important source of the equatorial metallic ions may be charge transfer reactions involving NO^+ and O_2^+ with the metal constituents, Mg and Fe. Strong depletions of NO^+ and O_2^+ at metallic ion peak heights in the night-time data combined with no apparent daytime photoionization enhancement of Mg^+ and Fe^+ appear to justify this interpretation.

Finally there is no evidence for perturbations in the distribution caused by the presence of the equatorial electrojet.

REFERENCES

- [1] Goldberg, R.A. and L.J. Blumle, J. Geophys. Res.,
75, 133, 1970.
- [2] Aikin, A.C., R.A. Goldberg, Y.V. Somayajulu, (1971)
in press.
- [3] Goldberg, R.A. and A.C. Aikin, NASA X-625-71-73, (1971)
in press.
- [4] Kane, J., NASA X-615-69-499, 1969.
- [5] Seddon, J.C., J. Geophys. Res., 58, 323, 1953.
- [6] Bauer, S.J., and J.E. Jackson, J. Brit. IRE, 23, 139,
1962.
- [7] Jackson, J.E., NASA X-625-71-154, 1971.
- [8] Narcisi, R.S., Trans. Am. Geophys. Union, 51, #4,
April 1970.
- [9] Narcisi, R.S. and W. Roth, Advances in Electronics
and Electron Physics, 29, 79, Academic Press Inc.,
New York, 1970.
- [10] Narcisi, R.S. and A.D. Bailey, J. Geophys. Res., 70,
3687, 1965.
- [11] Narcisi, R.S., Space Research, 8, 360, 1968.
- [12] Young, J.M., C.Y. Johnson and J.C. Holmes, J. Geophys.
Res., 72, 1473, 1967.
- [13] Awe, O., Proceedings of Upper Atmospheric Currents
and Electric Field Symposium, ESSA ERLTM-ESL, 12,
p. 52, 1970.

- [14] Swider, W., Jr., Planet. Space Sci., 17, 1233, 1969.
- [15] Maynard, N.C., L.J. Cahill, Jr. and T.S.G. Sastry,
J. Geophys. Res., 70, 1241, 1965.
- [16] Maynard, N.C. and L.J. Cahill, Jr., J. Geophys. Res.,
70, 5923, 1965.

FIGURE CAPTIONS

Figure 1 - Typical up and downleg raw spectra obtained from the ion mass spectrometer aboard 14.424.

Figure 2 - Current ratios indicating the relative contribution of heavy ionic constituents to the total current sampled.

Figure 3 - Comparison of D region ram and wake sampled absolute ion composition distributions from 14.424 data, $\chi = 27.8^\circ$.

Figure 4 - Comparison of D region ram and wake sampled absolute ion composition distributions from 14.425 data, $\chi = 53.2^\circ$.

Figure 5 - Comparison of the daytime E region ion composition at 8:27 and 10:17 LMT on March 19, 1970.

Figure 6 - Comparison of the nighttime E region ion composition at 19:38 and 1:08 LMT on March 9-10, 1970.

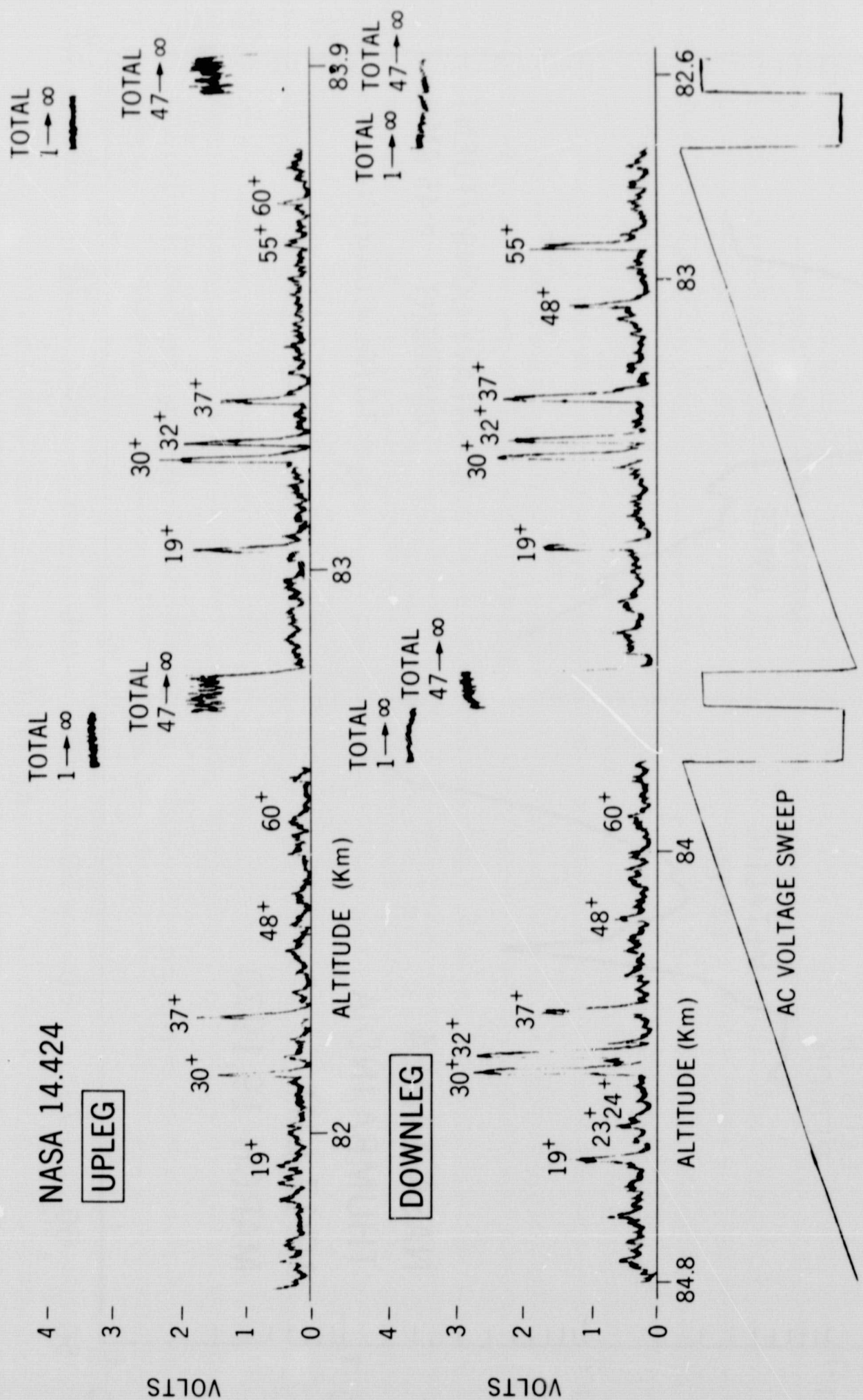


Figure 1

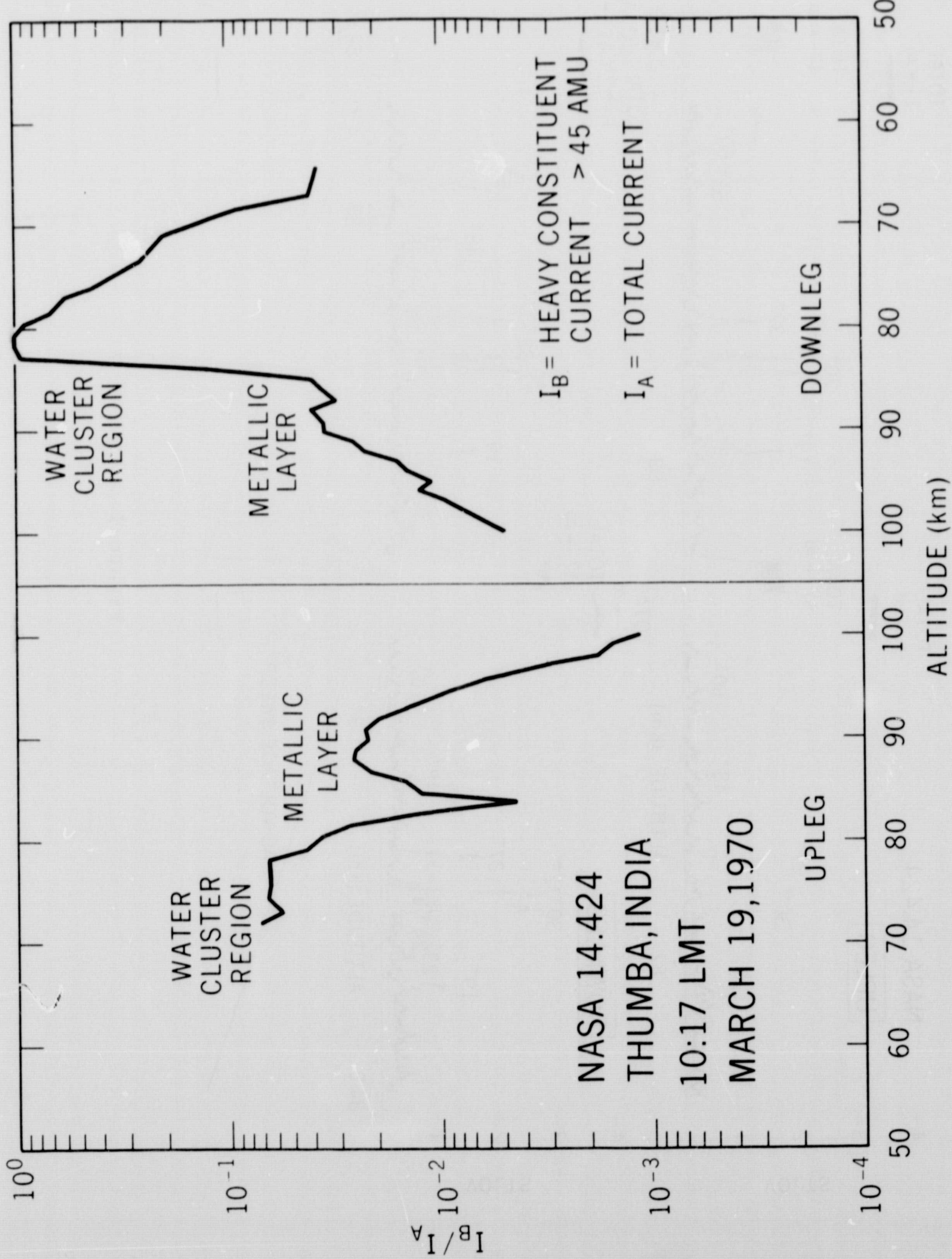


Figure 2

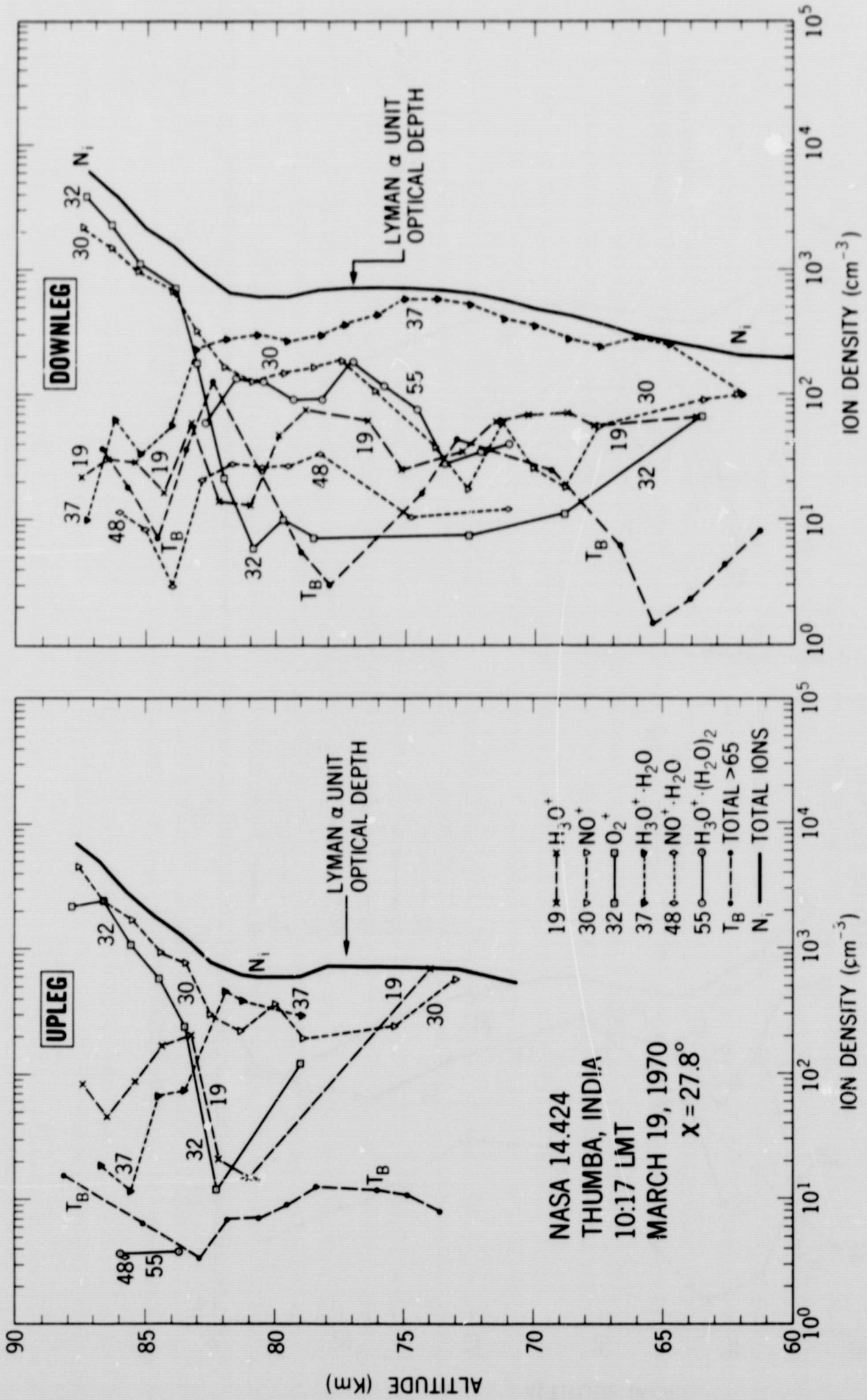


Figure 3

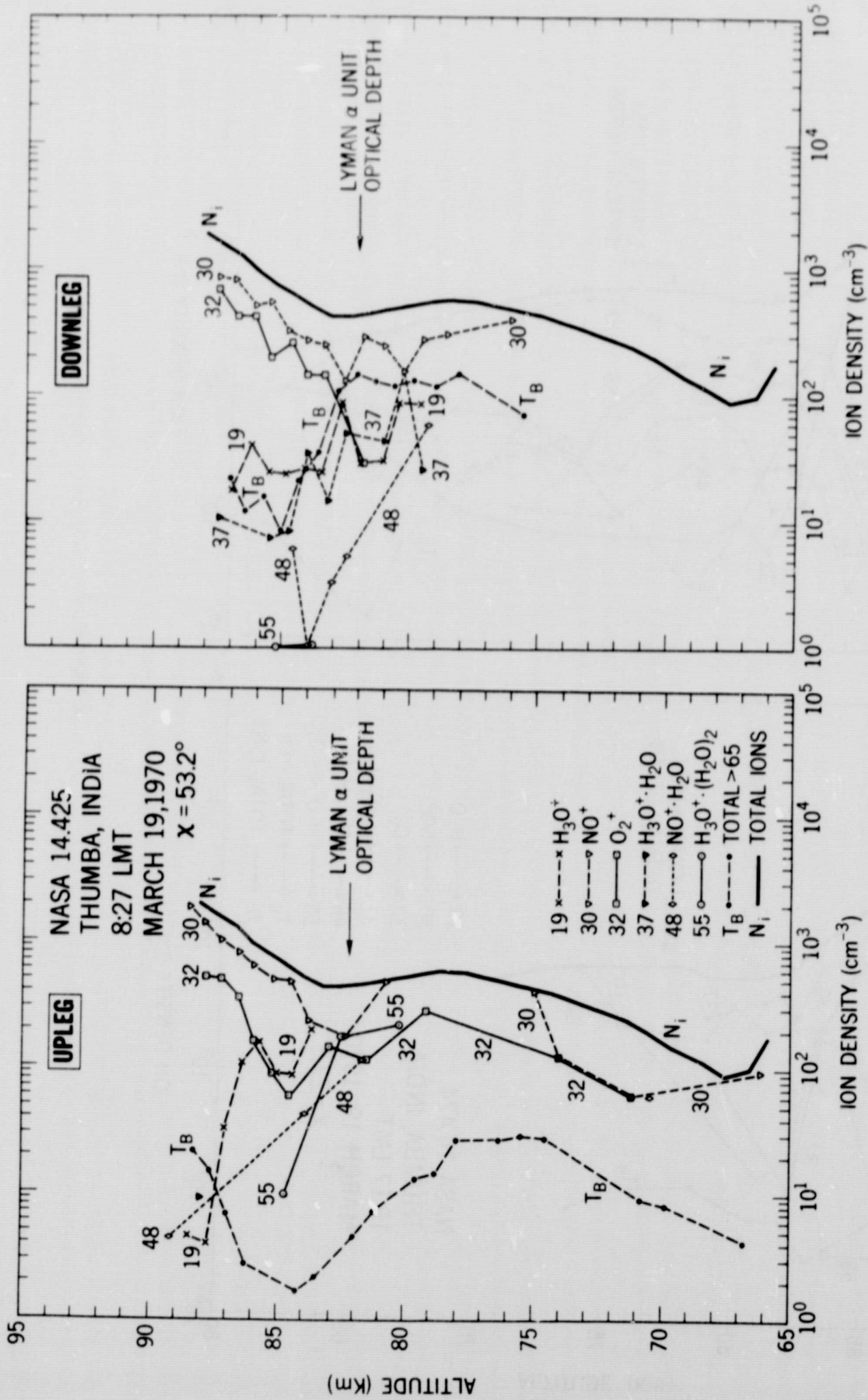
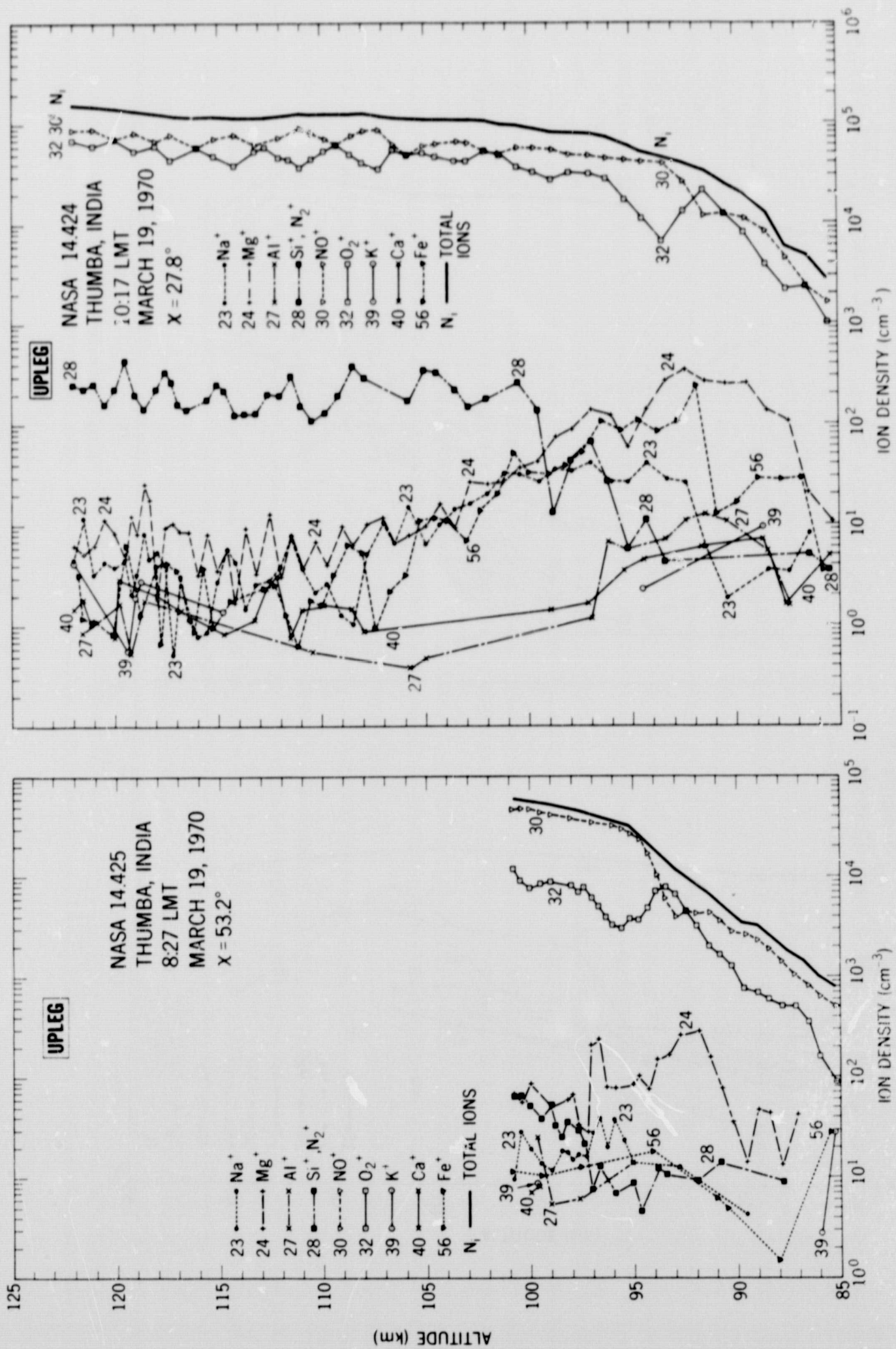


Figure 4

Figure 5



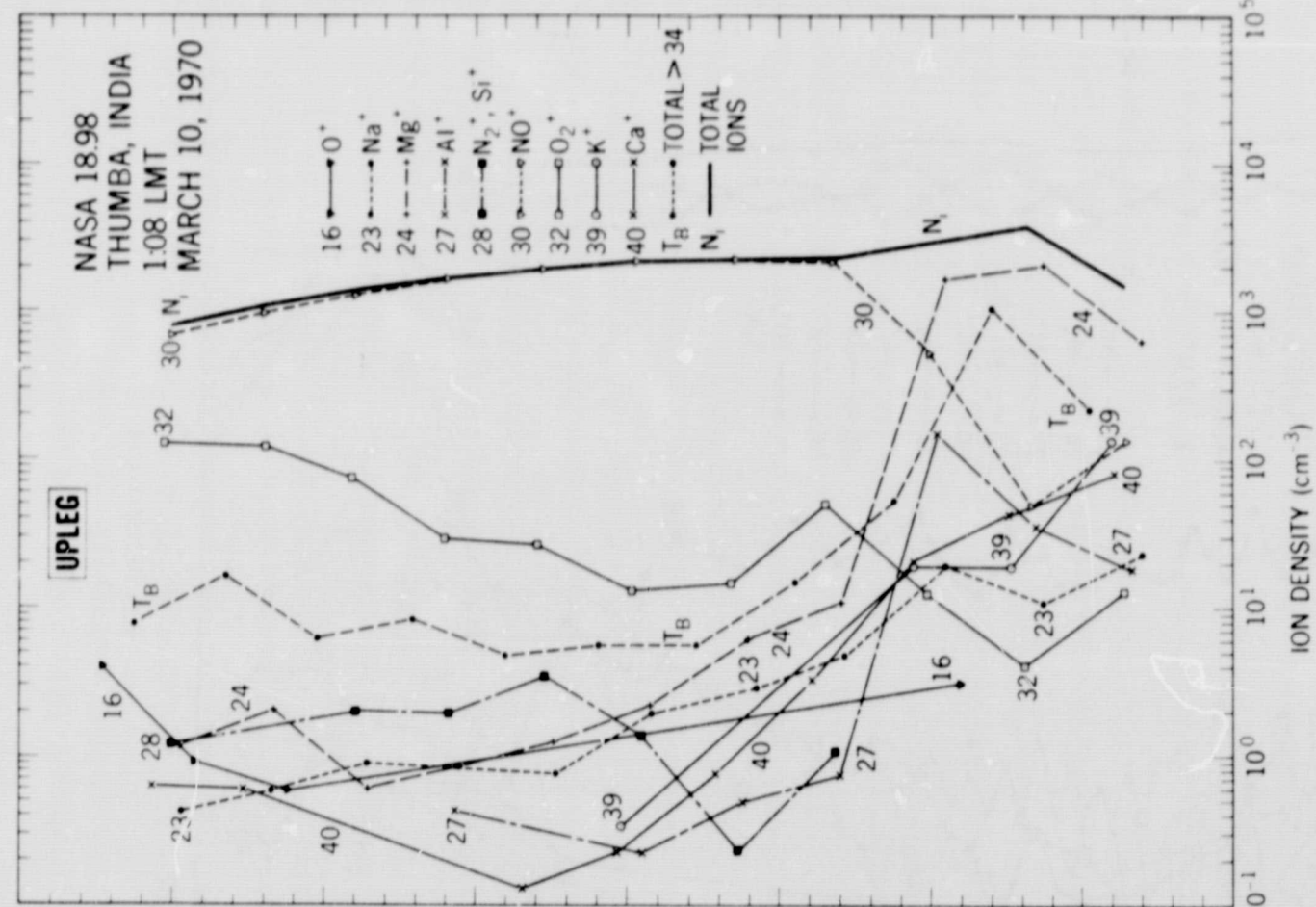
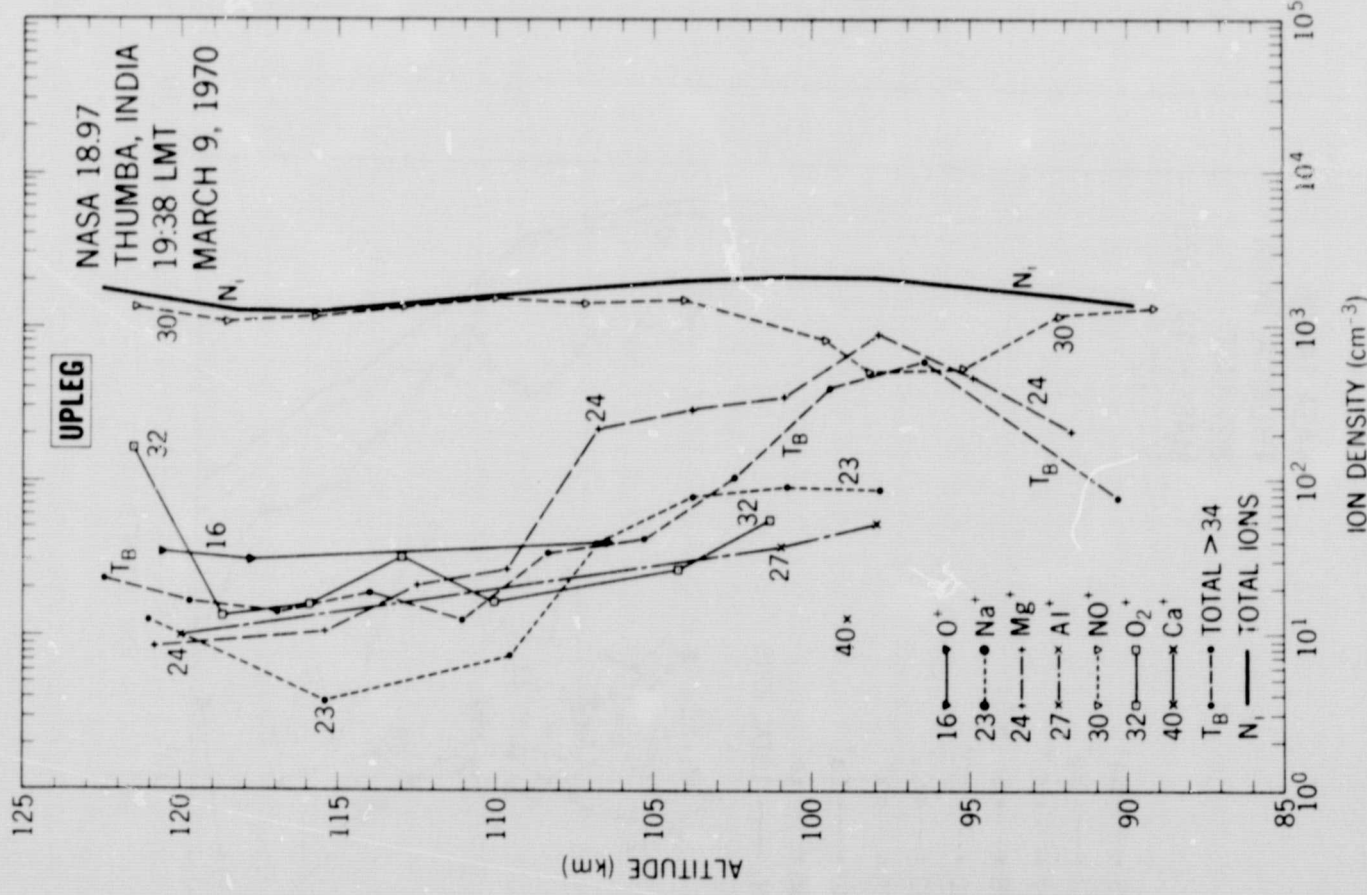


Figure 6